Title

Evidence for opposing roles of Celsr3 and Vangl2 in glutamatergic synapse formation

Journal

Proceedings of the National Academy of Sciences of the United States of America, 114(4)

ISSN

0027-8424

Authors

Thakar, Sonal
Wang, Liqing
Yu, Ting
et al.

Publication Date

2017-01-24

DOI

10.1073/pnas.1612062114

Peer reviewed

Evidence for opposing roles of Celsr3 and Vangl2 in glutamatergic synapse formation

Sonal Thakar[a], Liqing Wang[a], Ting Yu[a], Mao Ye[a], Keisuke Onishi[a], John Scott[a], Jiaxuan Qi[a], Catarina Fernandes[a], Xuemei Han[b], John R. Yates III[b], Darwin K. Berg[a], and Yimin Zou[a,1]

[a]Neurobiology Section, Biological Sciences Division, University of California, San Diego, La Jolla, CA 92093; and [b]Department of Chemical Physiology, The Scripps Research Institute, La Jolla, CA 92037

Edited by Liqun Luo, Stanford University, Stanford, CA, and approved December 5, 2016 (received for review July 22, 2016)

The signaling mechanisms that choreograph the assembly of the highly asymmetric pre- and postsynaptic structures are still poorly defined. Using synaptosome fractionation, immunostaining, and coimmunoprecipitation, we found that Celsr3 and Vangl2, core components of the planar cell polarity (PCP) pathway, are localized at developing glutamatergic synapses and interact with key synaptic proteins. Pyramidal neurons from the hippocampus of *Celsr3* knockout mice exhibit loss of ∼50% of glutamatergic synapses, but not inhibitory synapses, in culture. Wnts are known regulators of synapse formation, and our data reveal that Wnt5a inhibits glutamatergic synapses formed via Celsr3. To avoid affecting earlier developmental processes, such as axon guidance, we conditionally knocked out *Celsr3* in the hippocampus 1 week after birth. The CA1 neurons that lost *Celsr3* also showed a loss of ∼50% of glutamatergic synapses in vivo without affecting the inhibitory synapses assessed by miniature excitatory postsynaptic current (mEPSC) and electron microscopy. These animals displayed deficits in hippocampus-dependent behaviors in adulthood, including spatial learning and memory and fear conditioning. In contrast to *Celsr3* conditional knockouts, we found that the conditional knockout of *Vangl2* in the hippocampus 1 week after birth led to a large increase in synaptic density, as evaluated by mEPSC frequency and spine density. PCP signaling is mediated by multiple core components with antagonizing functions. Our results document the opposing roles of Celsr3 and Vangl2 in glutamatergic synapse formation.

Celsr3 | Vangl2 | glutamatergic | synapse formation

Glutamatergic synapses, the predominant excitatory synapses in the brain, are asymmetric cell–cell junctions formed from distinct pre- and postsynaptic components involving highly organized complexes of hundreds of proteins across the 20-nm synaptic cleft (1, 2). The signaling pathway that directly assembles these asymmetric protein complexes has not been well understood. Understanding mechanisms of glutamatergic synapse formation will provide important insights into the function and plasticity as well as dysfunction of glutamatergic synapses, which underlie numerous nervous system disorders.

Many epithelial tissues show planar cell polarity, the global asymmetry of cellular and tissue morphology and/or structure along the tissue plane (3, 4). The conserved core planar cell polarity (PCP) components, Frizzled, Dishevelled, Diego, Prickle, Vang(l), and Flamingo (Fmi)/Celsr, form asymmetric complexes at the cadherin-mediated adherens junctions that connect neighboring epithelial cells (3, 4). Recent studies suggest that mutations of some components of the PCP signaling pathway, *Celsr3*/*Fmi* and *Vangl2*, affect GABAergic circuit development in zebrafish retina, GABAergic motoneuron synapse development in *Caenorhabditis elegans*, and hippocampal/cortical glutamatergic and GABAergic synapse formation (5–11). PCP components are critical regulators of neuronal migration and axon guidance, which take place before synapse formation and their mutations may secondarily affect synapse formation (8–10, 12–19). Therefore, evaluating the specific functions of PCP components in synapse formation requires conditionally knocking out these components in defined synapses after the development of axons and dendrites.

In this study, we directly address the role of Celsr3 and Vangl2 in glutamatergic synapse formation by deleting *Celsr3* and *Vangl2* in hippocampal pyramidal neurons after the first postnatal week (postnatal day 7; P7). We found that at the peak of synapse formation (P14), Celsr3 and Vangl2 are specifically localized in developing glutamatergic synapses and colocalized with pre- and postsynaptic proteins. In the absence of *Celsr3*, hippocampal neurons showed ∼50% reduction in the number of glutamatergic synapses in vitro and in vivo. Inhibitory synapses were not affected. Noncanonical Wnt signaling inhibits glutamatergic synapse formation, whereas canonical Wnt signaling promotes glutamatergic synapse formation in the hippocampus (20). We found here that Celsr3, a key component of this noncanonical Wnt signaling pathway, the PCP pathway, mediates responses to Wnt5a, which negatively regulates synapse formation. Additionally, the postnatal deletion of *Celsr3* induced at P7 lead to deficits in hippocampus-dependent learning and memory formation. Some PCP components are known to exert opposing biochemical functions as well as exclude each other in subcellular localization. Indeed, we found that the postnatal deletion of *Vangl2* initiated at P7 resulted in an increase in glutamatergic synapses, measured at P14. Because mutations of some PCP components, such as Prickle1 and Prickle2, have been implicated in autism and epilepsy, precisely pinpointing the function of PCP signaling components will lead to better understanding of the synaptopathy underlying many neurological and neuropsychiatric disorders (21–24).

Results

Celsr3 and Vangl2 Are Localized in Excitatory Synapses. To characterize the role of Celsr3 and Vangl2 in developing synapses, we

Significance

The signaling mechanisms mediating glutamatergic synapse assembly are fundamental to our understanding of neural circuit function, plasticity, and disorders, but have remained elusive. We provide direct evidence that two components of the conserved planar cell polarity signaling pathway, which assembles asymmetric cell–cell junctions, have opposing functions in glutamatergic synapse formation. Celsr3 promotes assembly whereas Vangl2 inhibits assembly, suggesting that this signaling mechanism is accessible for both positive and negative regulation and is also a candidate pathway for mediating synaptic plasticity.

Author contributions: Y.Z. designed and directed research; S.T., L.W., T.Y., M.Y., K.O., J.S., J.Q., C.F., and X.H. performed research; S.T., L.W., T.Y., M.Y., K.O., J.S., J.R.Y., D.K.B., and Y.Z. analyzed data; and S.T. and Y.Z. wrote the paper.

The authors declare no conflict of interest.

This article is a PNAS Direct Submission.

[1]To whom correspondence should be addressed. Email: yzou@ucsd.edu.

This article contains supporting information online at www.pnas.org/lookup/suppl/doi:10.1073/pnas.1612062114/-/DCSupplemental.

focused on the glutamatergic synapses formed between the Schaffer collaterals and the hippocampal CA1 pyramidal neuron apical dendrites spanning the mouse stratum radiatum (Fig. 1*A*). This region is well characterized and a commonly used model for studying synapse formation. The onset of synaptogenesis occurs during the first postnatal week and continues for approximately 2 more weeks (Fig. 1*B*).

We first analyzed PCP components in the synaptic membrane fraction (SMF) and the postsynaptic density (PSD) using subcellular fractionation of synaptosome preparations from P14 wild-type mouse forebrains (Fig. 1*C*) (25, 26). As internal controls, synaptophysin and SV2, two presynaptic proteins, were examined and found enriched in the SMF, whereas PSD-95 and NMDA receptor subunit NR2B, two postsynaptic proteins, were enriched in the PSD fraction. We found that Celsr3 and Celsr2 were present in both fractions. Dvl1 was enriched in the SMF, whereas Dvl2 and Vangl2 were enriched in the PSD fraction. The hyperphosphorylated form of Fzd3 (top band) was more abundant in the SMF than in the PSD, whereas the unphosphorylated form of Fzd3 (bottom band) was enriched in the PSD fraction. This is consistent with our previous findings that Dvl1 increases hyperphosphorylation of Fzd3 to prevent its endocytosis and that Vangl2 and Dvl2 antagonize this by reducing Frizzled3 phosphorylation and promoting its internalization (14, 16). These results suggest that PCP components are asymmetrically localized at developing glutamatergic synapses in similar fashion to epithelial cell–cell junctions being planar polarized.

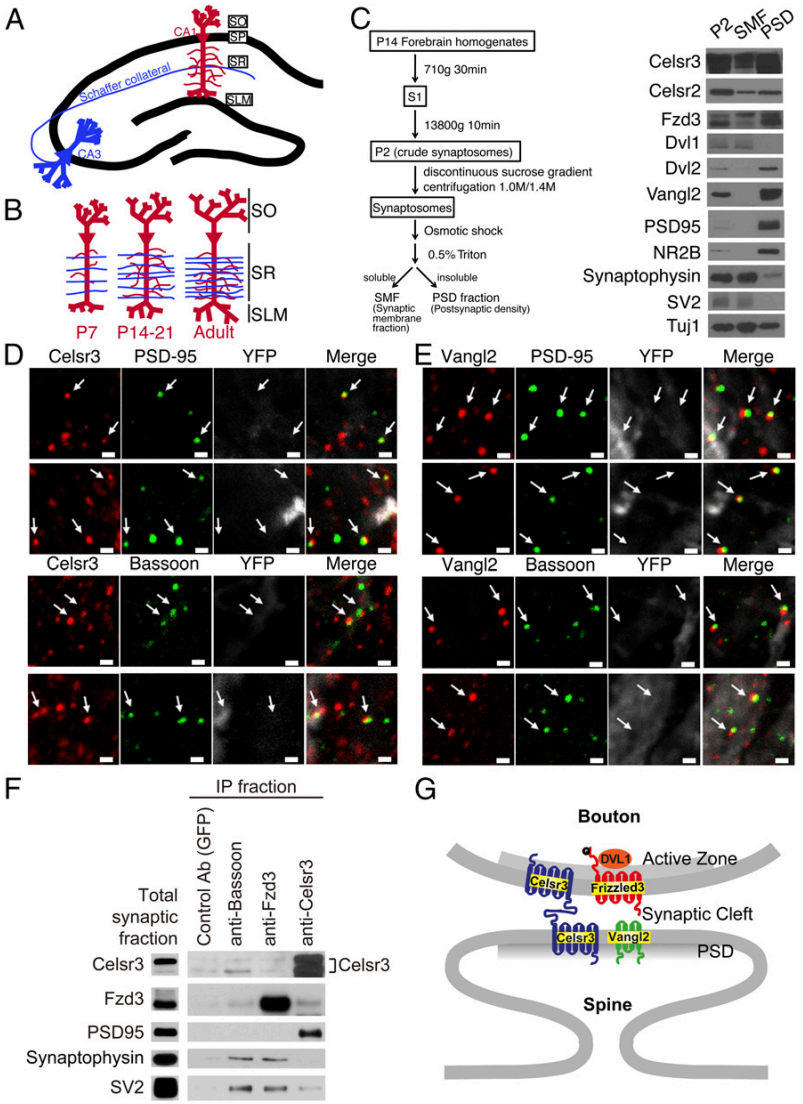

Fig. 1. PCP components are localized in developing excitatory synapses. (*A*) Schematic diagram of the CA3 to CA1 Schaffer collateral projections of the hippocampus. (*B*) Developmental progression of CA1 pyramidal neuron dendrites and CA3 axons. (*C*, *Left*) Diagram of the subcellular fractionation procedure. (*C*, *Right*) Western blot analysis of the distribution of PCP proteins by subcellular fractionation. P2, crude synaptosome; S1, supernatant. Tuj1 controls for loading. (*D* and *E*) Celsr3 (*D*) and Vangl2 (*E*) colocalization with postsynaptic marker PSD-95 and presynaptic marker bassoon. Arrows mark colocalized puncta in each image. (Scale bars, 1 μm.) (*F*) Immunoprecipitation (IP) assays using a P2 fraction of P14 wild-type mouse brains show interaction of endogenous Celsr3 and Frizzled3 proteins with endogenous synaptic proteins. (*G*) PCP components are distributed in glutamatergic synapses analogous to their organization in asymmetric epithelial cell junctions. SLM, stratum lacunosum moleculare; SO, stratum oriens; SP, stratum pyramidale; SR, stratum radiatum.

We then performed immunofluorescence staining of Celsr3 and Vangl2 in P14 hippocampal neurons in vivo. Celsr3 and Vangl2 were costained with either postsynaptic marker (PSD-95) or presynaptic marker (bassoon) on cryosections of hippocampus and visualized with confocal microscopy. We found at the peak of synaptogenesis that Celsr3 and Vangl2 are specifically colocalized in the developing synapses, as we observed colocalized puncta (denoted by arrows) of the Celsr3 and Vangl2 (red) puncta together with the synaptic marker (green) (Fig. 1 *D* and *E*). Although at the resolution of confocal microscopy it is not possible to separate the pre- and postsynaptic compartments, we observed highly specific colocalization (yellow) of these proteins together with the synaptic markers inside the synapses rather than distributed diffusely throughout the membranes of axons and dendrites. These results suggest that at this stage of postnatal development, Celsr3 and Vangl2 are likely specifically dedicated to regulating synapse formation. To visualize the dendrites and spines, we used a mouse line endogenously expressing yellow fluorescent protein (YFP) in the cytosol of a subset of CA1 pyramidal neurons (Fig. S1).

To test whether endogenous PCP components interact with specific synaptic proteins, we performed coimmunoprecipitation and Western blot using protein extracts from P14 mouse brain (Fig. 1*F*). After a series of centrifugation steps (26), the crude synaptosomal membrane pellet was solubilized and used for the coimmunoprecipitation. We found that endogenous Celsr3 interacts with SV2, PSD-95, and Frizzled3 (16), whereas endogenous Frizzled3 interacts with synaptophysin and SV2 (Fig. 1*F*). Recent studies also showed that other PCP proteins, Vangl2 and Prickle2, are found in the postsynaptic compartment and may interact with PSD-95 (5, 6). These data indicate that PCP components interact with a number of key synaptic proteins, suggesting a direct role in glutamatergic synapse assembly/function. The localization of PCP components and their interaction with key synaptic proteins are analogous to their organization in asymmetric epithelial cell junctions in PCP signaling (Fig. 1*G*).

***Celsr3* Is Required for Glutamatergic Synapse Formation in Hippocampal Culture.** To test the function of Celsr3 in synapse formation, we examined hippocampal neurons in 14-DIV (days in vitro) cultures prepared from embryonic day (E)18.5 *Celsr3* knockout mice (KOs) (27). Compared with wild-type (WT), $Celsr3^{-/-}$ cultures contained 24 ± 4% fewer presynaptic puncta as revealed by vGlut1 immunostaining, 36 ± 6.7% fewer postsynaptic puncta as revealed by PSD-95 staining, and 38 ± 5% fewer colocalized puncta characteristic of glutamatergic synapses (Fig. 2 *A* and *B*; $^{**}P < 0.01$ for pre- and postsynaptic puncta; $^{*}P < 0.05$ for colocalized puncta; Mann–Whitney *U*-statistic test). Knockout of *Celsr3* did not affect the mean area of the glutamatergic synapses marked by colocalized vGlut1+/PSD-95+ puncta (Fig. 2 *A* and *C*). No deficits were seen in the number or area of inhibitory synapses revealed by immunostaining $Celsr3^{-/-}$ cultures, indicating that inhibitory synapses are not regulated by Celsr3 (Fig. 2 *D*–*F*).

To assess the effects on early stages of synaptogenesis, we cultured E18.5 hippocampal neurons from $Celsr3^{-/-}$ embryos for only 6 days and examined synapse formation. We found that after 6 days of culture, when synapses are just beginning to form, the reduction of excitatory synapse puncta number was already significant (Fig. 2 *G* and *H*), suggesting that *Celsr3* is required at the onset of synapse formation. Although the areas of colocalized presynaptic vGlut1+ puncta were not different from the 14-DIV cultures (Fig. 2*C*), the areas of colocalized presynaptic vGlut1+ puncta were smaller in the 6-DIV cultures, further suggesting that Celsr3 is required for synapse assembly but not for maintenance. The areas of colocalized postsynaptic PSD-95+ puncta were unaffected in $Celsr3^{-/-}$ 6-DIV cultures (Fig. 2 *G* and *I*). The reduction in vGlut1+/PSD-95+ glutamatergic synapses as early as 6 DIV and persisting at least until 14 DIV provides evidence supporting the possible role of Celsr3 in glutamatergic synapse formation.

Wnt5a inhibits glutamatergic synapses formed by Celsr3. Previous studies have shown that Wnt signaling regulates synapse development in various neuronal cell types (28). Wnt5a is robustly expressed in the mouse hippocampus during postnatal development and reduces the number of presynaptic puncta in neurons via a noncanonical Wnt signaling pathway (20). Therefore, we sought to determine whether Celsr3 mediated Wnt5a signaling. Hippocampi isolated from E18 $Celsr3^{+/+}$ and $Celsr3^{-/-}$ mice were treated with Wnt5a after 12 DIV (100 ng/mL for 36 h). $Celsr3^{+/+}$ neurons showed a 56% reduction in the number of colocalized puncta (Fig. 2 *J* and *K*; $^{**}P < 0.01$, two-way ANOVA) at 14 DIV. $Celsr3^{-/-}$ neurons not treated with Wnt5a showed a 52% reduction compared with untreated $Celsr3^{+/+}$ neurons in colocalized puncta (Fig. 2 *J* and *K*; $^{**}P < 0.01$, two-way ANOVA). Wnt5a addition to $Celsr3^{-/-}$ neurons did not produce a significant difference compared with untreated $Celsr3^{-/-}$ neurons (Fig. 2 *J* and *K*), suggesting that Wnt5a inhibits synapse formation via a PCP component, Celsr3. To determine whether the reduction of synaptic puncta for vGlut1 and PSD-95 was due to changes in transcription, translation, or stability of these proteins, cell lystates for $Celsr3^{+/+}$ and $Celsr3^{-/-}$ cultured hippocampal neurons 14 DIV were collected to probe for vGlut1, PSD-95, vGAT, and gephyrin. There was no reduction in their total protein levels in $Celsr3^{-/-}$ (Fig. 2*L*).

***Celsr3* Is Required for Excitatory Synapse Formation in Vivo.** Because *Celsr3* is essential for axon guidance (12–14, 17, 18), it is critical to delete *Celsr3* after axons have reached their proper target area using *Celsr3* conditional knockout mice (cKOs) to test its role in synapse formation in vivo. We crossed a *Celsr3* cKO with an inducible Cre line (SLICK) so that we could delete *Celsr3* postnatally (12, 29). The SLICK-A line expresses constitutively active YFP and a tamoxifen-inducible form of Cre recombinase, $CreER^{T2}$, from two separate *Thy-1* promoters. The Thy-1 promoter of SLICK-A restricts Cre and YFP expression to neurons. There is no YFP fluorescence in glial cells, including GFAP+ astrocytes and Olig2+ oligodendrocytes or interneurons (29, 30). As a result, we can specifically assess the function of *Celsr3* in pyramidal neurons.

We first characterized the expression of YFP and the efficiency of recombination over the course of the first 2 postnatal weeks. SLICK-A is expressed in 59% of CA1 neurons indicated by the expression of YFP, and expressed sparsely in the cortex and other regions (Fig. S1*A*). In the absence of tamoxifen injections, SLICK-A–positive mice show no recombination at P7, although modest recombination at P14 due to a low level of leaky Cre expression (Fig. S1 *B* and *C*). However, administering tamoxifen at P7 to P8 resulted in robust recombination by P14, as indicated by 99% coexpression of tdTomato and YFP (Fig. S1 *A* and *D*–*F*; $n = 4$ mice, $n = 460$ neurons). For all of the in vivo experiments described below, control mice (SLICK-A–negative or SLICK-A–positive;$Celsr3^{+/+}$) were littermates and tamoxifen-injected at P7 and P8 and compared with tamoxifen-injected at P7 and P8 *Celsr3* cKOs (SLICK-A–positive;$Celsr3^{flox/flox}$). No changes were observed in the gross hippocampal anatomy, dendritic complexity, hippocampal commissure, mossy fiber projections, or CA1/CA3 cell-layer thickness and density, confirming that *Celsr3* was deleted late enough to avoid defects in axon guidance, neuronal migration, and dendrite morphogenesis (Fig. S1 *E*–*L*; control and *Celsr3* cKO, $n = 3$ mice). To characterize the cellular morphology, we analyzed dendritic complexity in the *Celsr3* cKOs by injecting Alexa Fluor hydrazide 555 into CA1 pyramidal cell bodies in acute hippocampal slices to label the

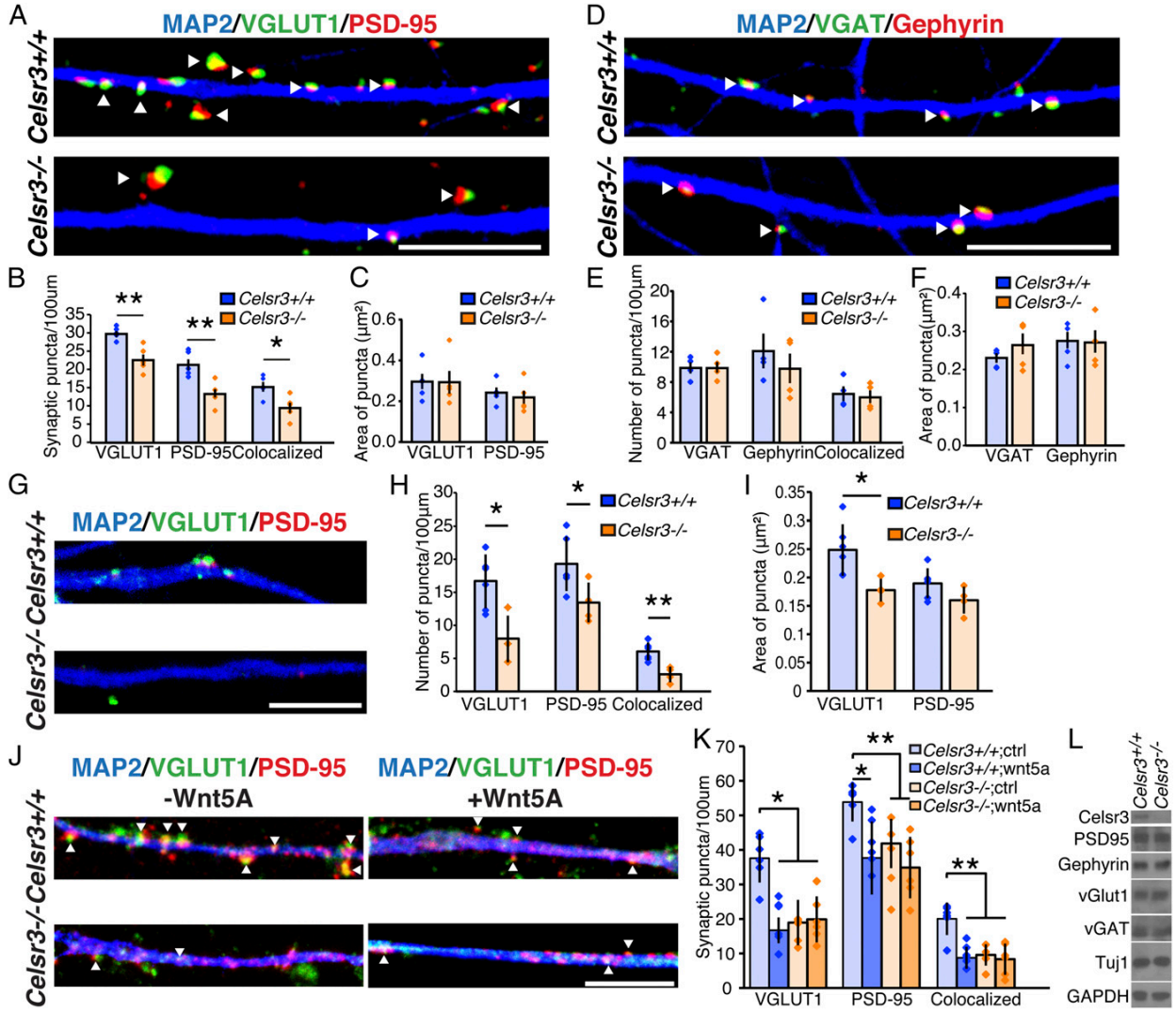

Fig. 2. *Celsr3* is required for glutamatergic synapse formation in hippocampal culture. (*A*) Immunostaining for pre- (green) and postsynaptic puncta (red) of glutamatergic synapses in 14-DIV hippocampal cultures from *Celsr3*$^{+/+}$ and *Celsr3*$^{-/-}$ E18.5 embryos. (*B* and *C*) Quantification of the density and area of glutamatergic synapses (*Celsr3*$^{+/+}$ $n = 5$ experiments, $n = 50$ neurons; *Celsr3*$^{-/-}$ $n = 5$ experiments, $n = 49$ neurons; $^{*}P < 0.05$, $^{**}P < 0.01$, Mann–Whitney *U*-statistic test). *Celsr3*$^{-/-}$ showed 24 ± 4%, 36 ± 6.7%, and 38 ± 5% reduction in presynaptic, postsynaptic, and colocalized puncta, respectively. The synaptic area was not significantly different. (*D*) Staining for pre- (green) and postsynaptic puncta (red) of inhibitory synapses in 14-DIV hippocampal cultures from *Celsr3*$^{+/+}$ or *Celsr3*$^{-/-}$ E18.5 embryos. (*E* and *F*) Quantification of the density and area of inhibitory synapses (*Celsr3*$^{+/+}$ $n = 4$ experiments, $n = 46$ neurons; *Celsr3*$^{-/-}$ $n = 4$ experiments, $n = 47$ neurons). Neither the density nor the area of inhibitory synapses was significantly different. (*G*) Staining for pre- (green) and postsynaptic puncta (red) of glutamatergic synapses in 6-DIV hippocampal cultures from *Celsr3*$^{+/+}$ and *Celsr3*$^{-/-}$ E18.5 hippocampal neurons. (*H* and *I*) Quantification of glutamatergic synaptic density showed a significant reduction in presynaptic, postsynaptic, and colocalized puncta. The area of postsynaptic puncta showed no change, whereas the area of presynaptic puncta showed a statistically significant change (*Celsr3*$^{+/+}$ $n = 127$ neurons, $n = 6$ experiments; *Celsr3*$^{-/-}$ $n = 85$ neurons, $n = 4$ experiments; $^{*}P < 0.05$, $^{**}P < 0.01$, Mann–Whitney *U*-statistic test). (*J*) Coimmunostaining for MAP2, PSD-95, and vGlut1 on *Celsr3*$^{+/+}$ or *Celsr3*$^{-/-}$ 14-DIV hippocampal neuronal dendrites after application of Wnt5a peptide. (*K*) Quantification of synaptic density after Wnt5a addition to *Celsr3*$^{+/+}$ or *Celsr3*$^{-/-}$ neurons. Colocalized vGlut1 and PSD-95 puncta density drops 56.4% after application of Wnt5a to *Celsr3*$^{+/+}$ neurons ($n = 6$ experiments; $^{*}P < 0.05$, $^{**}P < 0.01$, two-way ANOVA). *Celsr3*$^{-/-}$ neurons show a 52.2% decrease in the number of colocalized puncta compared with control neurons ($^{**}P < 0.01$, two-way ANOVA). No significant change is observed after the addition of Wnt5a to *Celsr3*$^{-/-}$ neurons. (*L*) There is no change in synaptic protein expression in *Celsr3*$^{-/-}$ compared with *Celsr3*$^{+/+}$ hippocampal cultures at 14 DIV. Arrowheads denote colocalized puncta. All data are expressed as mean ± SD. (Scale bars, 10 µm.)

entire cell body and dendritic branching pattern. Completely labeled neurons without artificially broken branches 200 µm from the soma were analyzed with Sholl analysis (ImageJ plugin). We found no significant difference between control and *Celsr3* cKO basal dendrites or apical dendrites spanning the stratum radiatum (Fig. S1 *M* and *N*; Student's *t* test at each 10-µm interval; control: $n = 11$ neurons, $n = 3$ mice; *Celsr3* cKO: n =10 neurons, $n = 3$ mice).

We performed electron microscopy (EM) to examine synaptic density on distal CA1 apical dendrites, 150 to 200 µm from pyramidal cell bodies in P14 littermates (tamoxifen-injected controls, and *Celsr3* cKOs on P7 and P8). Synapses in this region are

formed by the CA1 dendrites and Schaffer collateral fibers from CA3 pyramidal neurons (Fig. 1*A*). Images were taken at equally spaced regions spanning the stratum radiatum. Because 59% of the CA1 neurons expressed SLICK-A and 99% of the SLICK-A–positive neurons had undergone Cre recombination, *Celsr3* should be deleted in 58% of the CA1 neurons in tamoxifen-injected *Celsr3* cKO mice. We observed a significant 36% decrease (Fig. 3 *A* and *A′*; $^{*}P < 0.05$, Mann–Whitney *U*-statistic test) in the density of asymmetric (excitatory) axospinous synapses, whereas the density of asymmetric axodendritic synapses and symmetric (inhibitory) synapses remained unchanged (Fig. 3 *A–B′*). Due to the overlapping expression of Celsr2 with Celsr3 in hippocampal neurons (31, 32), we hypothesize that the remaining synapses in neurons lacking Celsr3 could be assembled by Celsr2 or a separate signaling pathway. These data show that Celsr3 is critical for the formation of excitatory synapses formed on spines and not the dendritic shaft or inhibitory synapses in vivo.

To assess the formation of functional synapses in vivo, we measured miniature excitatory postsynaptic current (mEPSC) and miniature inhibitory postsynaptic current (mIPSC) frequency and amplitude in acute hippocampal slices. Patch-clamp recordings of mEPSCs were obtained from CA1 pyramidal neurons of P13 to P15 littermates, tamoxifen-injected controls ($n = 20$ cells, $n = 7$ mice), and *Celsr3* cKOs ($n = 12$ cells, $n = 5$ mice) on P7 and P8 and in the presence of TTX (1 mM) and gabazine (10 μM). We found that loss of *Celsr3* caused a 45% reduction in the mean frequency of mEPSCs in CA1 neurons that express YFP (Fig. 3 *C* and *D*; $^{**}P = 0.0018$, Mann–Whitney *U*-statistic test), with no change in the mean mEPSC amplitude ($P = 0.77182$, Mann–Whitney *U*-statistic test) or decay time constant ($P = 0.42372$, Mann–Whitney *U*-statistic test) of the remaining synapses (Fig. 3 *C–E*). There were no significant changes in mIPSC frequency (control $n = 18$ cells, $n = 5$ mice; *Celsr3* cKO $n = 14$ cells, $n = 3$ mice; $P = 0.89656$, Mann–Whitney *U*-statistic test) or amplitude ($P = 0.72786$, Mann–Whitney *U*-statistic) or decay time constant ($P = 0.95216$, Mann–Whitney *U*-statistic test) (Fig. 3 *F–H*). These data indicate that Celsr3 plays a critical role in the development of excitatory, not inhibitory, synapses, contrary to previous studies that found embryonic loss of *Celsr3* also affected the formation of inhibitory synapses (10). The decrease in mEPSC frequency observed in the *Celsr3* cKO correlates with the observed decrease in excitatory synaptic density (asymmetric axospinous synapses) (Fig. 3 *A–B′*).

***Celsr3* Conditional Knockout Mice Display Impaired Hippocampus-Dependent Behaviors.** To test whether the reduction of excitatory synapse formation in the hippocampal CA1 pyramidal neurons resulted in behavioral deficits, we performed hippocampus-dependent behavioral tasks, including the Barnes maze and contextual fear conditioning (33, 34). Barnes maze tests were performed to evaluate hippocampus-dependent spatial memory in 3–4-month-old animals injected with tamoxifen at P7 and P8 (35). The Barnes maze consists of a circular field with 20 holes evenly spaced near its edge, one of which contains an escape route to a darkened escape chamber. Additional visual cues are placed on the wall for spatial orientation and a bright light is shined on the test area, giving the mouse an incentive to escape quickly. Because the maze does not involve water, it avoids complications due to the poorer swimming ability of mice (36). After initial habituation to the escape route and test area, the animals were subjected to four daily training sessions to form a stable memory of the location of the escape hole, followed by a probe test where the escape was removed.

We evaluated the latency to the first encounter of the escape hole by quantifying the latency to locate the hole with the escape chamber under it (37, 38). The controls had a significant learning curve (Fig. 4*A*; $P = 0.0022$, ANOVA, $n = 18$ male mice), whereas the *Celsr3* cKOs only had a trend toward a learning curve (Fig. 4*A*; $P = 0.0830$, ANOVA, $n = 17$ male mice). In addition, the controls had a significantly shorter latency to locate the hole with the escape chamber compared with *Celsr3* cKOs (Fig. 4*A*; $P = 0.0113$, ANOVA). These data suggest that *Celsr3* cKOs had impaired learning and memory in a hippocampus-dependent behavioral task.

In the probe test, control mice spent significantly more time in the quadrant originally housing the escape chamber than in the average of the other three quadrants, as expected (Fig. 4*B*; $^{*}P = 0.016$, ANOVA), indicating that they were correctly remembering spatial cues in this test. On the other hand, the difference in percent time spent in the target vs. the average of the other quadrants was not statistically significant in *Celsr3* cKOs (Fig. 4*B*; $P = 0.54$, ANOVA), indicating that *Celsr3* cKOs had impaired spatial memory.

The mice were then subjected to a fear-conditioning paradigm that evaluates context- and cue-dependent learning. Because the fear-conditioning test sometimes has adverse effects on other behavioral tests, the fear-conditioning test was the final behavioral test performed on the mice, after the Barnes maze and the control behavioral tests. The strong aversive foot-shock stimulus provides a robust learning and memory motivation and behavioral response. Contextual-fear conditioning is a hippocampus- and amygdala-dependent behavior, whereas cued-fear conditioning is an amygdala-dependent behavior (39, 40). In this experimental paradigm, freezing behavior—which was defined as the absence of all except respiratory movement—is quantified after mice learn to associate context (the chamber environment) and a conditioned stimulus (a previously neutral tone stimulus) with an aversive foot shock. After initial habituation, mice are placed in the context of the chamber and exposed to the condition of a buzzer alarm sound/light in association with the aversive foot-shock stimulus. The next day, mice were submitted to the context test, in which mice were placed in the same chamber but in the absence of the tone, light, and aversive foot shock. On the final day, the cued stimulus test was performed, in which the mice were placed in a novel chamber exposed to the light and tone in the absence of the aversive foot shock. The *Celsr3* cKOs displayed significantly weaker contextual conditioning compared with controls, which depends on hippocampal inputs (Fig. 4*C*; $^{*}P = 0.0491$, ANOVA), whereas cued-fear conditioning was completely intact (Fig. 4*C*; $P = 0.8825$). These data suggest *Celsr3* cKOs have a specific hippocampus-dependent behavioral defect.

Because SLICK-A is highly expressed in the hippocampus compared with other brain regions, including the cortex, at the time of tamoxifen injection (Fig. S1*A*), we expected behavioral defects would be restricted to those that are hippocampus-dependent. Indeed, there were no differences between control and *Celsr3* cKOs in visual function as measured in the optomotor test, in anxiety-like behavior as measured using the light/dark transfer test, or in activity levels assessed in the locomotor activity test (Fig. 4 *D–J*).

Vangl2 Inhibits Excitatory Synapse Formation in Vivo. The localized expression of Vangl2 protein in the postsynaptic density suggests a role in synapse formation. However, Vangl2 is also an important signaling component in axon guidance. Germline *Vangl2* mutations, either complete loss-of-function or gain-of-function (*looptail*), lead to massive axon projection defects (as well as other earlier developmental defects, such as an open neural tube), which will secondarily cause synapse formation defects (14, 41, 42). In two earlier studies, these germline *Vangl2* mutants show a decrease in dendritic complexity and spine density (7, 11). To identify the biological function of Vangl2 in synapse formation, which occurs postnatally, we crossed a *Vangl2* cKO allele (43) with the SLICK-A Cre line to delete *Vangl2* postnatally. To evaluate the role of *Vangl2* in functional synapses in vivo, we first measured mEPSC frequency and amplitude in acute hippocampal slices. Patch-clamp recordings of mEPSCs for P14 to P21 controls ($n = 17$ neurons, $n = 7$ mice) and *Vangl2* cKOs ($n = 18$ neurons, $n = 6$ mice) were performed the same way as for *Celsr3* cKO acute slices. In contrast to the germline *Vangl2* mutations, we observed a large,

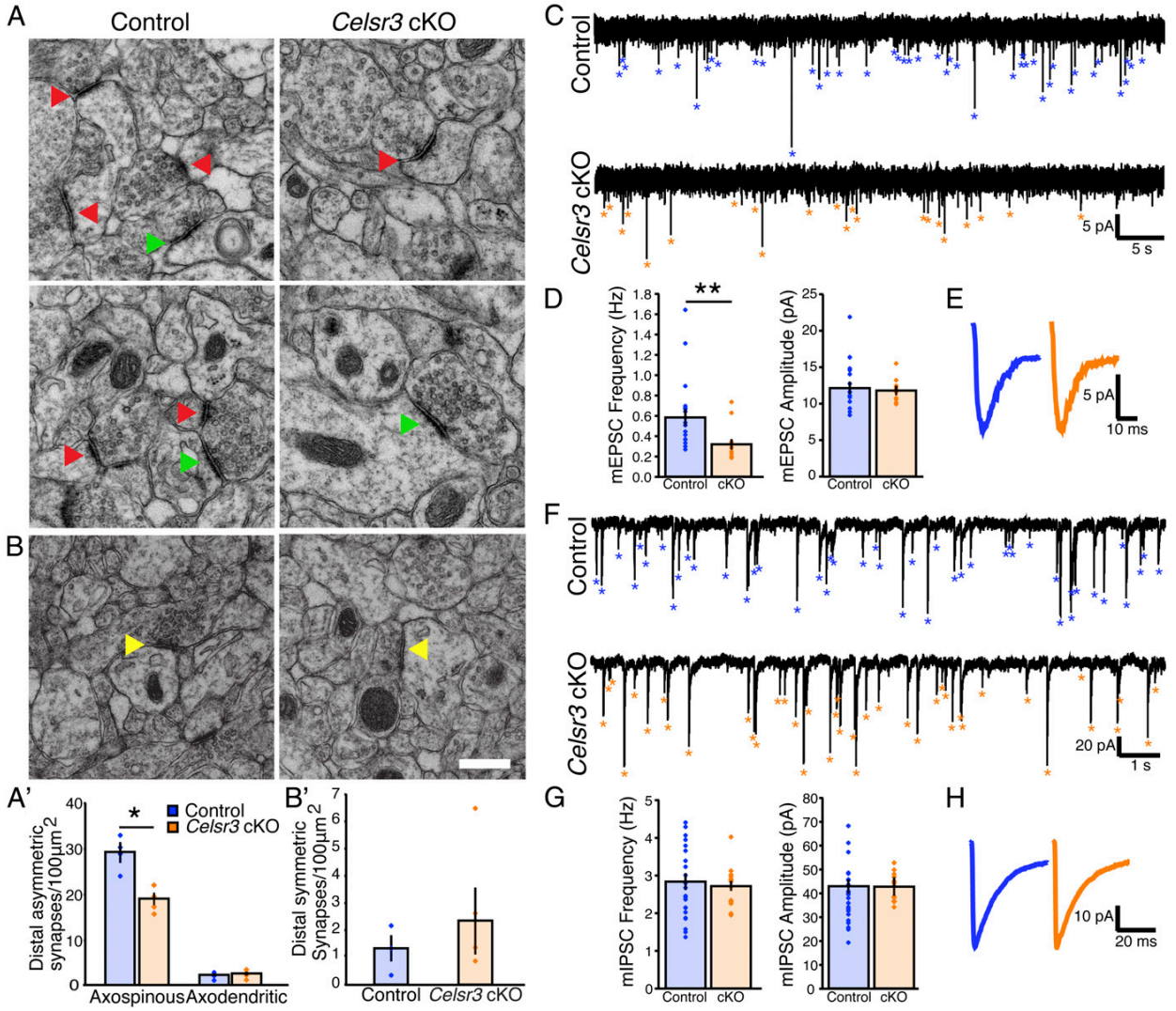

Fig. 3. *Celsr3* is required for excitatory synapse formation in vivo. (*A–B'*) Representative EM images and quantification showing a 36% decrease in distal asymmetric axospinous synaptic density (indicated by red arrowheads) on the apical CA1 dendrites in the stratum radiatum of *Celsr3* cKOs. Controls and *Celsr3* cKOs ($n = 4$ mice per group; $^{*}P < 0.05$, Mann–Whitney *U*-statistic test). There was no significant change in axodendritic synaptic density (indicated by green arrowheads) or in distal symmetric synaptic density (indicated by yellow arrowheads). (Scale bar, 400 nm.) (*C*) Representative traces showing mEPSCs (control, blue asterisks; cKO, orange asterisks). (*D*) Quantification of mean mEPSC frequency (*Left*) and amplitude (*Right*) recorded in control ($n = 20$ cells, $n = 7$ mice) and *Celsr3* cKO littermates ($n = 12$ cells, $n = 5$ mice) ($^{**}P < 0.01$, Mann–Whitney *U*-statistic test). (*E*) Average event trace for control and *Celsr3* cKO shows no significant difference in decay time constant ($P = 0.42372$, Mann–Whitney *U*-statistic test) of the remaining synapses. (*F*) Representative traces showing mIPSCs (control, blue asterisks; cKO, orange asterisks) recorded in CA1 hippocampal pyramidal neurons from controls (*Upper*) or *Celsr3* cKOs (*Lower*). (*G*) Quantification of mean mIPSC frequency (*Left*) and amplitude (*Right*) recorded in control ($n = 18$ cells, $n = 5$ mice) and cKO littermates ($n = 14$ cells, $n = 3$ mice) shows no significant difference. (*H*) Average event trace for control and *Celsr3* cKO shows no significant difference in decay time constant ($P = 0.95216$, Mann–Whitney *U*-statistic test). All data are expressed as mean ± SEM.

58% increase in the mean mEPSC frequency (Fig. 5 *A* and *B*; $^{**}P = 0.00252$, Mann–Whitney *U*-statistic test) with no change in the mean mEPSC amplitude (Fig. 5 *A* and *B*) or decay time constant (Fig. 5*C*; $P = 0.50286$, Mann–Whitney *U*-statistic test). Recording of the mIPSCs (control $n = 13$ neurons, $n = 3$ mice; *Vangl2* cKO $n = 11$ neurons, $n = 3$ mice) was performed and revealed no significant changes in mIPSC mean frequency (Fig. 5 *D* and *E*; $P = 0.45326$, Mann–Whitney *U*-statistic test), amplitude (Fig. 5 *D* and *E*; $P = 0.48392$, Mann–Whitney *U*-statistic test), or decay time constant (Fig. 5*F*; $P = 0.47152$, Mann–Whitney *U*-statistic test). These data suggest Vangl2 inhibits excitatory synapse formation.

We then analyzed spine density and morphology in P14 slices. Spines are dynamic structures that rapidly respond to environmental cues and molecular signaling. To preserve the spine density and morphology as close to the live mouse as possible, mice were anesthetized and quickly transcardially perfused with room temperature 4% paraformaldehyde (PFA). After processing the tissue (44), CA1 neurons and their dendritic branches were injected with Alexa Fluor hydrazide 555 to visualize spines. Only YFP+ neurons were included in the analysis, to ensure Cre-expressing dendrites were evaluated in the SLICK-A+;*Vangl2* cKO. CA1 oblique apical dendrites located 100 to 200 μm from

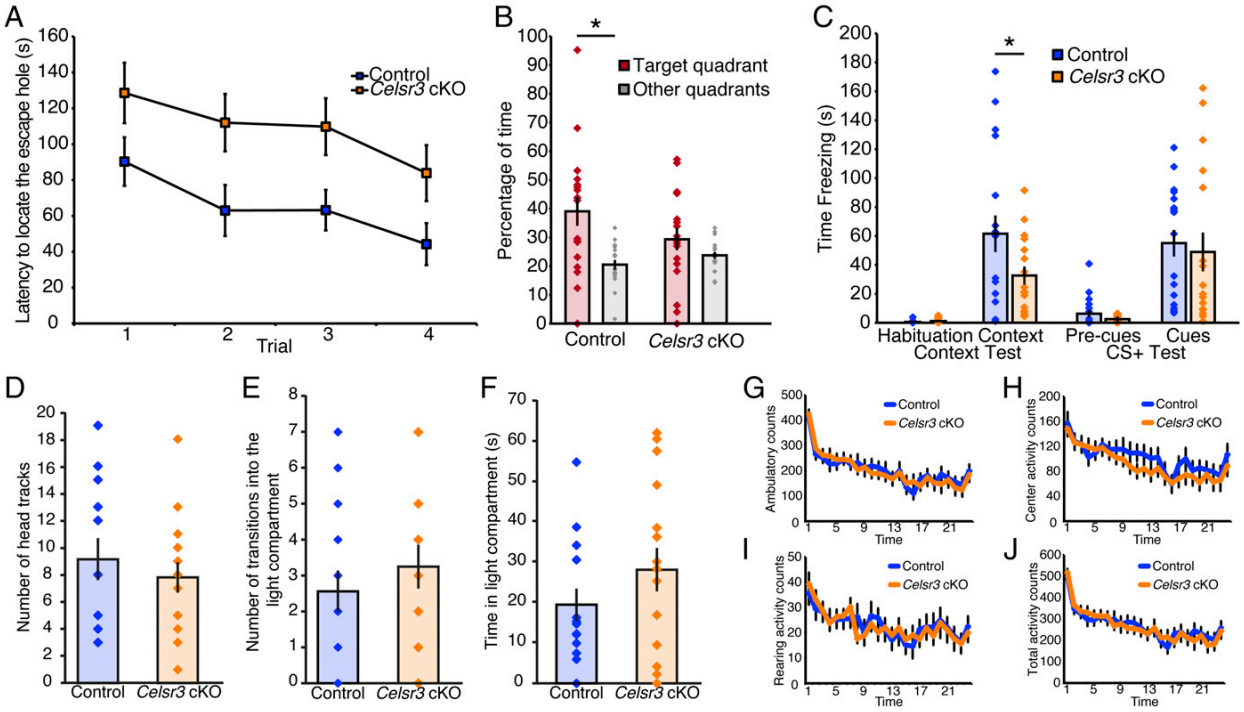

Fig. 4. *Celsr3* conditional knockout mice displayed impaired hippocampus-dependent behaviors. (*A*) *Celsr3* cKO littermates showed a longer latency in locating the escape chamber than control littermates in the Barnes maze assay (control $n = 18$; cKO $n = 17$; $P = 0.0113$, ANOVA). The controls had a significant learning curve ($n = 18$ male mice; $P = 0.0022$, ANOVA), whereas the *Celsr3* cKOs only showed a trend toward a learning curve ($n = 17$ male mice; $P = 0.0830$, ANOVA). (*B*) In the probe test, control mice spent significantly more time in the quadrant originally housing the escape chamber than the average of the other three quadrants [$F(1,17) = 7.14$, $^{*}P = 0.016$, ANOVA]. *Celsr3* cKOs showed no significant difference in the percent time spent in the target vs. other quadrants [$F(1,15) = 0.40$, $P = 0.54$, ANOVA]. (*C*) *Celsr3* cKOs had significant impairment of hippocampus-dependent contextual conditioning ($^{*}P < 0.05$, unpaired Student's *t* test) as reflected by the 50% reduced time spent freezing in the fear conditioning test. Hippocampus-independent cued conditioning remained the same. (*D–J*) Behavioral tests for non–hippocampus-dependent tasks showed no differences between control and *Celsr3* cKO mice as observed in (*D*) visual ability in the optomotor test, (*E* and *F*) anxiety-like behavior as measured using the light/dark transfer test, or (*G–J*) activity levels assessed in the locomotor activity test. All data are expressed as mean ± SEM.

the CA1 pyramidal neuronal cell bodies spanning the stratum radiatum were imaged using confocal microscopy, and spine density and morphology were analyzed. *Vangl2* cKO lead to 29% increase of spine density (Fig. 5*G*; 15.6 ± 0.06 spines per 10-μm dendritic segment; $n = 24$ neurons, $n = 4$ mice; $^{***}P < 0.001$, Student's *t* test) compared with controls (Fig. 5*G*; 12.1 ± 0.04 spines per 10-μm dendritic segment; $n = 31$ neurons, $n = 3$ mice). The average percentage of stubby-shaped spines in *Vangl2* cKOs decreased by 36% (Fig. 5*G*; $^{***}P < 0.001$, Student's *t* test) and the average percentage of thin-shaped spines increased by 18% (Fig. 5*G*; $^{**}P = 0.00104$, Student's *t* test). The increase in mEPSC frequency observed in the *Vangl2* cKO correlates with the increase in excitatory synaptic density (as observed with quantifying spine density) in the *Vangl2* cKO. Together, these data suggest Vangl2 normally inhibits initial spine formation and potentially indirectly or directly promotes spine elimination, contrary to previous reports (7, 11).

Discussion

Opposing Roles of Celsr3 and Vangl2 in Glutamatergic Synapse Formation. We found that PCP components are specifically localized at excitatory synapses as they form during early postnatal development and are associated either directly or indirectly with a number of key synaptic proteins. Hippocampal neurons lacking *Celsr3* develop approximately half as many excitatory synapses, as revealed by immunostaining, electron microscopy, and patch-clamp recording of mEPSCs both in cultured hippocampal neurons and in acute hippocampal slices. Both the *Celsr3* KO and cKO showed no change in the number of inhibitory synapses, and the *Celsr3* cKO displayed no change in the activity of inhibitory synapses. The remaining excitatory synapses after the loss of *Celsr3* may be formed by other *Celsr* isoforms, such as Celsr2 expressed in an overlapping pattern in the hippocampus (31, 32), or a separate signaling pathway. These synaptic defects manifested in hippocampus-dependent behavioral deficits in adult *Celsr3* cKOs. Therefore, this study precisely identifies the essential role of a core PCP protein, Celsr3, in glutamatergic synapse formation. Because PCP components often have opposing functions and mutually exclusive subcellular localization, we anticipated that if PCP-like signaling is responsible for synapse formation, there should be some components that will inhibit synapse formation. Indeed, we found that Vangl2 inhibits glutamatergic synapse formation in the same hippocampal pyramidal neurons. Our paper provides evidence that components of the PCP signaling pathway have opposing functions in glutamatergic synapse formation, suggesting that PCP signaling mediates both positive and negative regulation of synapse formation and may be a candidate for a novel regulatory mechanism of synaptic plasticity.

Direct Role of Celsr3 and Vangl2 in Synapse Formation. Because PCP signaling components play important roles in multiple steps of neural development, including neuronal migration and axon guidance, the proper experimental design is required to precisely dissect the function of each component and assign their role in

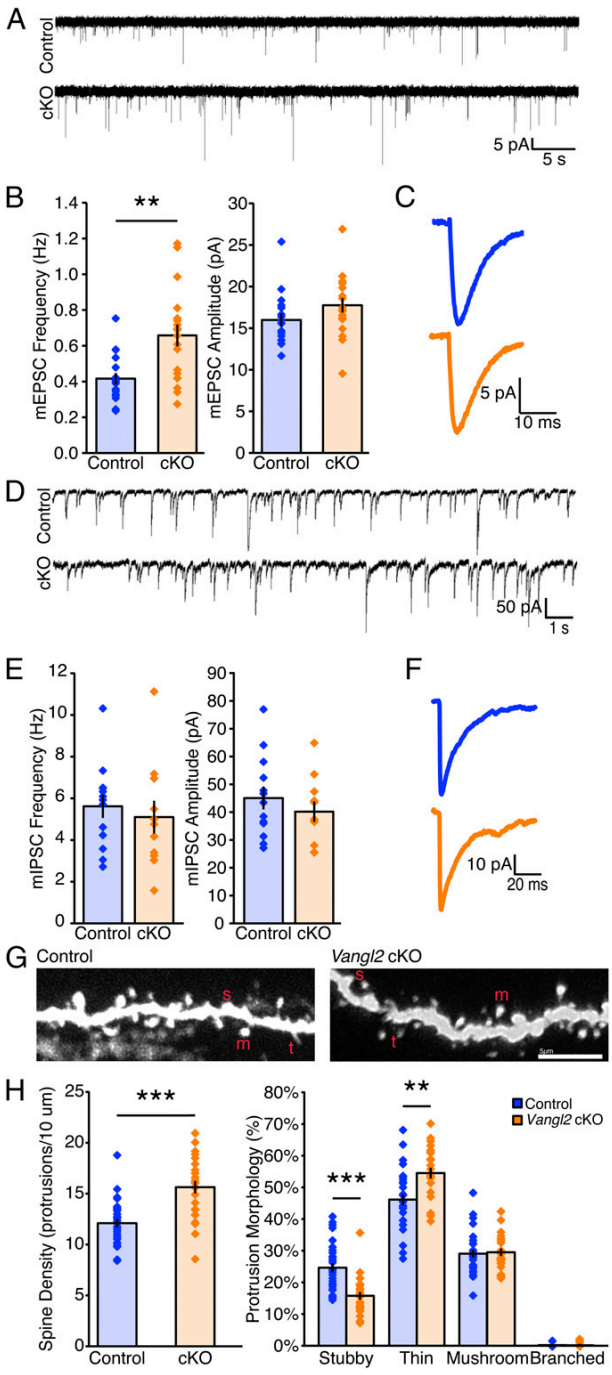

Fig. 5. *Vangl2* inhibits excitatory synapse formation in vivo. (*A*) Representative traces showing mEPSCs. (*B*) Quantification of mean mEPSC frequency (*Left*) and amplitude (*Right*) recorded in control ($n = 17$ cells, $n = 7$ mice) and *Vangl2* cKO littermates ($n = 18$ cells, $n = 6$ mice; $^{**}P < 0.01$, Mann–Whitney *U*-statistic test). (*C*) Average event trace for control and *Vangl2* cKO shows no significant difference in decay time constant ($P = 0.50286$, Mann–Whitney *U*-statistic test). (*D*) Representative traces showing mIPSCs recorded in CA1 hippocampal pyramidal neurons from controls (*Upper*) or *Vangl2* cKOs (*Lower*). (*E*) Quantification of mean mIPSC frequency (*Left*) and amplitude (*Right*) recorded in control ($n = 13$ cells, $n = 3$ mice) and *Vangl2* cKO littermates ($n = 11$ cells, $n = 3$ mice) shows no significant difference. (*F*) Average event trace for control and cKO shows no significant difference in decay time constant ($P = 0.47152$, Mann–Whitney *U*-statistic test). (*G*) Representative images of control and *Vangl2* cKO dendritic spines from P16 CA1 neurons labeled by cell filling with Alexa Fluor 555 hydrazide. m, mushroom; s, stubby; t, thin. (Scale bar, 5 μm.) (*H*) *Vangl2* cKO has a significant 29% increase in average spine density ($^{***}P < 0.001$, Student's *t* test). cKO has a significant 36% decrease in stubby-shaped spines ($^{***}P < 0.001$, Student's *t* test) and an 18% increase in thin-shaped spines ($^{**}P < 0.01$, Student's *t* test). All data are expressed as mean ± SEM.

synapse formation (12–18). Previous studies deleted the *Celsr3* gene either from early embryonic development or early embryonic brain development (8–10). When *Celsr3* was deleted from the embryonic forebrain using *Emx1-Cre*, a number of defects were found in neuronal cell numbers, migration, and axon guidance. These severe early defects will have an impact on later phases of development, such as synapse formation, which rely on correct axon guidance and dendrite formation. In addition to the reduction of glutamatergic synapses, inhibitory synapse numbers were found to be increased, probably due to the cell migration and axon guidance defects (10). In our study, *Celsr3* was deleted postnatally and we observed no change in tissue/cellular arrangement or axon guidance, therefore avoiding the early developmental confounds and allowing us to analyze the precise role of *Celsr3* in synapse formation. We did not observe any changes in inhibitory/symmetric synapse formation, consistent with our observation that Celsr3 and Vangl2 were not present in symmetric synapses. Similarly, another recent study implicated Vangl2 in glutamatergic synapse formation using the *looptail* mouse line containing a germline point mutation in the *Vangl2* gene (7). The authors found that Vangl2 binds to N-cadherin and promotes the endocytosis of N-cadherin, suggesting that Vangl2 normally disassembles synapses because N-cadherin promotes synapse formation. However, glutamatergic synapse formation was found to be greatly reduced using the *looptail* heterozygous mutant. The *looptail* mouse line has a point mutation in the *Vangl2* gene, which is embryonic-lethal in homozygotes, and heterozygotes show a number of severe neural developmental defects, including open neural tube, neurogenesis, neuronal migration, and axon guidance defects (14, 41). Therefore, the reduction of glutamatergic synapse formation is probably secondary to these earlier defects, misrepresenting the true function of Vangl2. Furthermore, the *looptail* mutation has been proposed to be a gain-of-function mutation, which could lead to other unexpected artifacts (42). Therefore, our study correctly assigns the function of Celsr3 and Vangl2 in glutamatergic synapse formation, laying down the foundation for future studies in this important pathway for synapse formation and potentially plasticity.

Wnt signaling has long been implicated in synapse formation (28). However, due to the complexity of Wnt signaling mechanisms, some published papers may report apparently conflicting results. In our study, we show that the Celsr3-mediated signaling pathway responds to the inhibitory function of Wnt5a in glutamatergic synapse formation. We also revealed the opposing roles of Wnt-regulated PCP components, Celsr3 and Vangl2, in glutamatergic synapse formation. Therefore, the precise function of Celsr3 and Vangl2 in synapse formation that we report here will provide important clues to fully understand the mechanisms of the assembly and plasticity of glutamatergic synapses in health and disease.

Materials and Methods

Celsr3 KO and cKO mice were provided by Andre Goffinet, Université Catholique de Louvain, Brussels (12, 13). *Vangl2* cKO mice were provided by Yingzi Yang, Harvard Medical School (43). The SLICK-A (JAX; 007606) line (29) constitutively expresses YFP and expresses a tamoxifen-inducible form of Cre recombinase, $CreER^{T2}$. P7 and P8 pups were administered tamoxifen via intraperitoneal injection once daily. All experiments were performed with littermate, tamoxifen-injected controls. All animal work in this research was approved by the University of California, San Diego (UCSD) Institutional Animal Care and Use Committee.

Subcellular fractionation and coimmunoprecipitation data were collected from P14 wild-type mouse brains. All hippocampal culture data are from E18.5 embryos collected from littermate *Celsr3* KO mice (*Celsr3*$^{+/+}$ and *Celsr3*$^{-/-}$). Celsr3 and Vangl2 immunofluorescence staining was performed at P14 in SLICK-A–positive; *Celsr3*$^{+/+}$ mice. *Celsr3* cKO EM was performed in P14 mice imaging the CA1 apical dendrites 150 to 200 μm from the cell body spanning the stratum radiatum. *Celsr3* cKO and *Vangl2* cKO mEPSC and mIPSC recordings were from acute hippocampal slices taken from 2- to 3-week-old mice. *Vangl2* cKOs were from mice that were killed and perfused at room temperature and then neurons individually labeled using Alexa Fluor hydrazide 555 (Invitrogen). All behavioral experiments were performed in mice 3 to 4 months old. Additional details regarding methods for all experiments described here are available in *SI Materials and Methods*.

ACKNOWLEDGMENTS. We thank Massimo Scanziani for initial help with electrophysiology experiments. We thank the Electron Microscopy Core Facility at the UCSD School of Medicine for access to their electron microscope and tissue preparation facilities, and the Mouse Behavioral Assessment Core at The Scripps Research Institute for behavioral tests. This project was supported by Grants NS047484, MH099082, and a March of Dimes grant (to Y.Z.), NIH Training Grant fellowships [Award T32 NS007220-27 and 2014 NARSAD Young Investigator Award (to S.T.); Award T32 GM007240-36 (to J.S.)], a Japan Society for Promotion of Sciences fellowship (to K.O.), Grant NS012601 (to D.K.B.), and the National Center for Research Resources (Grant 5P41RR011823-17) and National Institute of General Medical Sciences (Grant 8 P41 GM103533-17) (to J.R.Y.).

1. Sheng M, Kim E (2011) The postsynaptic organization of synapses. *Cold Spring Harb Perspect Biol* 3(12):a005678.
2. Südhof TC (2012) The presynaptic active zone. *Neuron* 75(1):11–25.
3. Wang Y, Nathans J (2007) Tissue/planar cell polarity in vertebrates: New insights and new questions. *Development* 134(4):647–658.
4. Zallen JA (2007) Planar polarity and tissue morphogenesis. *Cell* 129(6):1051–1063.
5. Hida Y, et al. (2011) Prickle2 is localized in the postsynaptic density and interacts with PSD-95 and NMDA receptors in the brain. *J Biochem* 149(6):693–700.
6. Yoshioka T, Hagiwara A, Hida Y, Ohtsuka T (2013) Vangl2, the planar cell polarity protein, is complexed with postsynaptic density protein PSD-95 [corrected]. *FEBS Lett* 587(10):1453–1459.
7. Nagaoka T, et al. (2014) The Wnt/planar cell polarity pathway component Vangl2 induces synapse formation through direct control of N-cadherin. *Cell Reports* 6(5):916–927.
8. Lewis A, et al. (2011) Celsr3 is required for normal development of GABA circuits in the inner retina. *PLoS Genet* 7(8):e1002239.
9. Najarro EH, et al. (2012) *Caenorhabditis elegans* flamingo cadherin fmi-1 regulates GABAergic neuronal development. *J Neurosci* 32(12):4196–4211.
10. Feng J, et al. (2012) A role for atypical cadherin Celsr3 in hippocampal maturation and connectivity. *J Neurosci* 32(40):13729–13743.
11. Okerlund ND, Stanley RE, Cheyette BN (2016) The planar cell polarity transmembrane protein Vangl2 promotes dendrite, spine and glutamatergic synapse formation in the mammalian forebrain. *Mol Neuropsychiatry* 2(2):107–114.
12. Zhou L, et al. (2008) Early forebrain wiring: Genetic dissection using conditional Celsr3 mutant mice. *Science* 320(5878):946–949.
13. Tissir F, Bar I, Jossin Y, De Backer O, Goffinet AM (2005) Protocadherin Celsr3 is crucial in axonal tract development. *Nat Neurosci* 8(4):451–457.
14. Shafer B, Onishi K, Lo C, Colakoglu G, Zou Y (2011) Vangl2 promotes Wnt/planar cell polarity-like signaling by antagonizing Dvl1-mediated feedback inhibition in growth cone guidance. *Dev Cell* 20(2):177–191.
15. Qu Y, et al. (2010) Atypical cadherins Celsr1-3 differentially regulate migration of facial branchiomotor neurons in mice. *J Neurosci* 30(28):9392–9401.
16. Onishi K, et al. (2013) Antagonistic functions of Dishevelleds regulate Frizzled3 endocytosis via filopodia tips in Wnt-mediated growth cone guidance. *J Neurosci* 33(49):19071–19085.
17. Fenstermaker AG, et al. (2010) Wnt/planar cell polarity signaling controls the anterior-posterior organization of monoaminergic axons in the brainstem. *J Neurosci* 30(47):16053–16064.
18. Shima Y, et al. (2007) Opposing roles in neurite growth control by two seven-pass transmembrane cadherins. *Nat Neurosci* 10(8):963–969.
19. Onishi K, Hollis E, Zou Y (2014) Axon guidance and injury—Lessons from Wnts and Wnt signaling. *Curr Opin Neurobiol* 27:232–240.
20. Davis EK, Zou Y, Ghosh A (2008) Wnts acting through canonical and noncanonical signaling pathways exert opposite effects on hippocampal synapse formation. *Neural Dev* 3:32.
21. Bassuk AG, et al. (2008) A homozygous mutation in human PRICKLE1 causes an autosomal-recessive progressive myoclonus epilepsy-ataxia syndrome. *Am J Hum Genet* 83(5):572–581.
22. Tao H, et al. (2011) Mutations in prickle orthologs cause seizures in flies, mice, and humans. *Am J Hum Genet* 88(2):138–149.
23. Sowers LP, et al. (2013) Disruption of the non-canonical Wnt gene PRICKLE2 leads to autism-like behaviors with evidence for hippocampal synaptic dysfunction. *Mol Psychiatry* 18(10):1077–1089.
24. Paemka L, et al. (2013) PRICKLE1 interaction with SYNAPSIN I reveals a role in autism spectrum disorders. *PLoS One* 8(12):e80737.
25. Cohen RS, Blomberg F, Berzins K, Siekevitz P (1977) The structure of postsynaptic densities isolated from dog cerebral cortex. I. Overall morphology and protein composition. *J Cell Biol* 74(1):181–203.
26. Hallett PJ, Collins TL, Standaert DG, Dunah AW (2008) Biochemical fractionation of brain tissue for studies of receptor distribution and trafficking. *Curr Protoc Neurosci* 42(Unit 1.16):1–16.
27. Meffert MK, Chang JM, Wiltgen BJ, Fanselow MS, Baltimore D (2003) NF-kappa B functions in synaptic signaling and behavior. *Nat Neurosci* 6(10):1072–1078.
28. Salinas PC, Zou Y (2008) Wnt signaling in neural circuit assembly. *Annu Rev Neurosci* 31:339–358.
29. Young P, et al. (2008) Single-neuron labeling with inducible Cre-mediated knockout in transgenic mice. *Nat Neurosci* 11(6):721–728.
30. Heimer-McGinn V, Young P (2011) Efficient inducible Pan-neuronal cre-mediated recombination in SLICK-H transgenic mice. *Genesis* 49(12):942–949.
31. Allen Institute (2015) *Allen Developing Mouse Brain Atlas* (Allen Inst Brain Sci, Seattle).
32. Loh KH, et al. (2016) Proteomic analysis of unbounded cellular compartments: Synaptic clefts. *Cell* 166(5):1295–1307.e21.
33. Blundell J, et al. (2010) Neuroligin-1 deletion results in impaired spatial memory and increased repetitive behavior. *J Neurosci* 30(6):2115–2129.
34. Carmona MA, Murai KK, Wang L, Roberts AJ, Pasquale EB (2009) Glial ephrin-A3 regulates hippocampal dendritic spine morphology and glutamate transport. *Proc Natl Acad Sci USA* 106(30):12524–12529.
35. Barnes CA (1979) Memory deficits associated with senescence: A neurophysiological and behavioral study in the rat. *J Comp Physiol Psychol* 93(1):74–104.
36. Whishaw IQ, Tomie J (1996) Of mice and mazes: Similarities between mice and rats on dry land but not water mazes. *Physiol Behav* 60(5):1191–1197.
37. Patil SS, Sunyer B, Höger H, Lubec G (2009) Evaluation of spatial memory of C57BL/6J and CD1 mice in the Barnes maze, the multiple T-maze and in the Morris water maze. *Behav Brain Res* 198(1):58–68.
38. Harrison FE, Reiserer RS, Tomarken AJ, McDonald MP (2006) Spatial and nonspatial escape strategies in the Barnes maze. *Learn Mem* 13(6):809–819.
39. Phillips RG, LeDoux JE (1992) Differential contribution of amygdala and hippocampus to cued and contextual fear conditioning. *Behav Neurosci* 106(2):274–285.
40. Maren S, Yap SA, Goosens KA (2001) The amygdala is essential for the development of neuronal plasticity in the medial geniculate nucleus during auditory fear conditioning in rats. *J Neurosci* 21(6):RC135.
41. Torban E, Wang HJ, Groulx N, Gros P (2004) Independent mutations in mouse Vangl2 that cause neural tube defects in looptail mice impair interaction with members of the Dishevelled family. *J Biol Chem* 279(50):52703–52713.
42. Yin H, Copley CO, Goodrich LV, Deans MR (2012) Comparison of phenotypes between different vangl2 mutants demonstrates dominant effects of the Looptail mutation during hair cell development. *PLoS One* 7(2):e31988.
43. Song H, et al. (2010) Planar cell polarity breaks bilateral symmetry by controlling ciliary positioning. *Nature* 466(7304):378–382.
44. Dumitriu D, Rodriguez A, Morrison JH (2011) High-throughput, detailed, cell-specific neuroanatomy of dendritic spines using microinjection and confocal microscopy. *Nat Protoc* 6(9):1391–1411.
45. Wessel D, Flügge UI (1984) A method for the quantitative recovery of protein in dilute solution in the presence of detergents and lipids. *Anal Biochem* 138(1):141–143.
46. Ippolito DM, Eroglu C (2010) Quantifying synapses: An immunocytochemistry-based assay to quantify synapse number. *J Vis Exp* 45:e2270.
47. Christopherson KS, et al. (2005) Thrombospondins are astrocyte-secreted proteins that promote CNS synaptogenesis. *Cell* 120(3):421–433.
48. Bach ME, Hawkins RD, Osman M, Kandel ER, Mayford M (1995) Impairment of spatial but not contextual memory in CaMKII mutant mice with a selective loss of hippocampal LTP in the range of the theta frequency. *Cell* 81(6):905–915.
49. Holmes A, Wrenn CC, Harris AP, Thayer KE, Crawley JN (2002) Behavioral profiles of inbred strains on novel olfactory, spatial and emotional tests for reference memory in mice. *Genes Brain Behav* 1(1):55–69.
50. Paylor R, Zhao Y, Libbey M, Westphal H, Crawley JN (2001) Learning impairments and motor dysfunctions in adult Lhx5-deficient mice displaying hippocampal disorganization. *Physiol Behav* 73(5):781–792.
51. Maren S (2001) Neurobiology of Pavlovian fear conditioning. *Annu Rev Neurosci* 24:897–931.
52. Rudy JW, Huff NC, Matus-Amat P (2004) Understanding contextual fear conditioning: Insights from a two-process model. *Neurosci Biobehav Rev* 28(7):675–685.
53. Kenney JW, Gould TJ (2008) Nicotine enhances context learning but not context-shock associative learning. *Behav Neurosci* 122(5):1158–1165.
54. Harris KM, Jensen FE, Tsao B (1992) Three-dimensional structure of dendritic spines and synapses in rat hippocampus (CA1) at postnatal day 15 and adult ages: Implications for the maturation of synaptic physiology and long-term potentiation. *J Neurosci* 12(7):2685–2705.
55. Bochner DN, et al. (2014) Blocking PirB up-regulates spines and functional synapses to unlock visual cortical plasticity and facilitate recovery from amblyopia. *Sci Transl Med* 6(258):258ra140.
56. Vogel-Ciernia A, et al. (2013) The neuron-specific chromatin regulatory subunit BAF53b is necessary for synaptic plasticity and memory. *Nat Neurosci* 16(5):552–561.
57. Tang G, et al. (2014) Loss of mTOR-dependent macroautophagy causes autistic-like synaptic pruning deficits. *Neuron* 83(5):1131–1143.
58. Jiang M, et al. (2013) Dendritic arborization and spine dynamics are abnormal in the mouse model of MECP2 duplication syndrome. *J Neurosci* 33(50):19518–19533.
59. Calfa G, et al. (2012) HDAC activity is required for BDNF to increase quantal neurotransmitter release and dendritic spine density in CA1 pyramidal neurons. *Hippocampus* 22(7):1493–1500.
60. Moser EI, Kropff E, Moser MB (2008) Place cells, grid cells, and the brain's spatial representation system. *Annu Rev Neurosci* 31:69–89.